



Intertwined magnetization and exchange bias reversals across compensation temperature in YbCrO_3 compound

Deepak, A. Kumar, and S. M. Yusuf 

*Solid State Physics Division, Bhabha Atomic Research Centre, Mumbai, 400085, India
and Homi Bhabha National Institute, Anushaktinagar, Mumbai 400094, India*

 (Received 9 June 2021; revised 8 October 2021; accepted 2 November 2021; published 2 December 2021)

We have investigated the origin of magnetization and exchange bias (EB) reversals in the YbCrO_3 compound at the magnetization compensation temperature, T_{COMP} of 16.5 K by dc magnetization, ac susceptibility, neutron diffraction (ND), neutron depolarization, specific heat, and dielectric measurements. A weak magnetization (M_{Cr}) is observed below the Néel temperature T_{N} (~ 120 K) in dc magnetization, which is consistent with a canted antiferromagnetic (AFM) state due to ordering of Cr^{3+} moments. Specific heat data exhibit a λ -shaped peak at T_{N} . Further, a monotonic increase of ac susceptibility at low temperatures and the Schottky anomaly in the specific heat data account for the polarized nature of the Yb^{3+} moment (M_{Yb}) under the molecular field of the AFM Cr^{3+} sublattice. Our ND study has confirmed a finite polarized Yb^{3+} ordered moment, and the G_z -type AFM ordering of Cr^{3+} moments below T_{N} . The temperature variations of the lattice constants a and b show a crossover from positive to negative thermal expansion (NTE) across the T_{COMP} while cooling. Below T_{COMP} , the separation between Cr-Cr atoms lying in the ab plane increases with decrease in temperature, which corroborates with the observed NTE of the lattice constants. In the present compound, the sign change of the net magnetization arising out of the AFM coupled polarized Yb^{3+} (M_{Yb}) and the ferromagnetic Cr^{3+} (M_{Cr}) sublattice moments results in the sign reversal of magnetization. Interestingly, anomalous behavior of the coercive field with its minimum value at $T \sim T_{\text{COMP}}$ is observed. EB also changes sign at $T \sim T_{\text{COMP}}$. Moreover, the temperature variation of the real part of the dielectric constant reveals an anomaly at T_{COMP} , indicating a weak magnetodielectric coupling in the YbCrO_3 compound. A training effect analysis ensures the conventional nature of the observed EB. Neutron depolarization study sheds light on the temperature-dependent domain magnetization with its zero value at the T_{COMP} . The presence of the observed important phenomena viz. magnetization and EB reversals in a single-phase compound suggests their possible use in making magnetization switching, spin-value, thermomagnetic, and other spintronic devices.

DOI: [10.1103/PhysRevMaterials.5.124402](https://doi.org/10.1103/PhysRevMaterials.5.124402)

I. INTRODUCTION

The rare earth chromites $R\text{CrO}_3$, where R is a rare earth element, have continued to be a focus of research in the last few decades due to their interesting applications in spintronic devices, solid oxide fuel cells, multiferroics, and thermo-electric devices [1]. These materials crystallize in the orthorhombic crystal structure with four formula units per unit cell. In orthochromites, depending upon the rare earth element, Cr^{3+} sublattice usually orders at the Néel temperature ($T_{\text{N}} \sim 112\text{--}288$ K [2]) into a canted antiferromagnetic (AFM) structure with a small ferromagnetic (FM) component of moment; however, R^{3+} sublattice orders in the liquid helium temperature range. In some systems, the rare earth element does not order and remains in the paramagnetic (PM) state down to 2 K [3]. The interaction between ordered Cr^{3+} and the ordered/polarized R^{3+} sublattice moment can produce various interesting phenomena, such as negative magnetization (NM) [1] and exchange bias (EB) [4]. The NM [also called magnetization reversal (MR)] is a phenomenon

in which net dc magnetization of a system under a constant magnetic field changes its sign from a positive to a negative value at a certain temperature, called compensation temperature (T_{COMP}) and is found in several single-phase magnetic systems [1]. Whereas EB is a phenomenon in which isothermal $M(H)$ hysteresis loop shifts along the horizontal magnetic field axis from its normal symmetric position when the system is cooled under some magnetic field through the T_{N} of the material. In the literature, EB has been reported in various heterogeneous magnetic systems such as core-shell nanoparticles ($\text{BiFe}_{0.8}\text{Mn}_{0.2}\text{O}_3$ [5], $\text{BiFeO}_3/\text{NiFe}_2\text{O}_4$ [6], and $\text{La}_{0.2}\text{Ce}_{0.8}\text{CrO}_3$ [7]), FM/spin-glass systems [8], and FM/AFM multilayers [9]. Some systems exhibit positive EB (PEB) and some negative EB (NEB), but the sign reversal from a positive to a negative value under the effect of external parameters such as temperature and cooling magnetic field is rare and is mainly found in some heterogeneous systems [8] and intermetallic compounds [10]. Recent studies have shown that several bulk homogeneous systems such as NdMnO_3 [11,12], $\text{YFe}_{0.5}\text{Cr}_{0.5}\text{O}_3$ [13], TmCrO_3 [14,15], and $\text{Gd}_{1-x}\text{Y}_x\text{CrO}_3$ [16] exhibit both sign reversal of magnetization and EB across the T_{COMP} with varying temperature and magnetic field, where different types of mechanisms play

*smyusuf@barc.gov.in

a role. For example, in NdMnO_3 , exchange coupling between Nd and canted Mn ordered moments was responsible for observed sign reversal of magnetization and EB phenomena. In $\text{YFe}_{0.5}\text{Cr}_{0.5}\text{O}_3$, coexistence of NM and EB was explained by competition between Dzyaloshinskii-Moriya interaction and single-ion magnetocrystalline anisotropy. In $\text{TmCrO}_3/\text{Gd}_{1-x}\text{Y}_x\text{CrO}_3$, exchange interaction between the polarized moment of Tm/Gd sublattice and the canted Cr moment was responsible for these two phenomena. Although the cause of NM and EB is different in different systems, these systems have one common feature: all are AFM-dominating systems with a weak FM moment. Additionally, all these systems have >1 magnetic ion at the same or different sublattices. The systems showing sign reversal of magnetization have important applications in making thermomagnetic switches, and the sign reversal of EB across the T_{COMP} could be exploited to make thermally assisted magnetic random access memory [17]. In this paper, we focus on the magnetic rare-earth-based perovskite compound YbCrO_3 .

The reported macroscopic dc magnetization data on bulk [18–20], nanoparticle [21], and single-crystal [22] of YbCrO_3 compound reveal that magnetic phase transition occurs at $T_N \sim 120$ K. These magnetic studies on YbCrO_3 also reveal that the compound exhibits NM with T_{COMP} ranging from ~ 16.5 to 19 K and a sign reversal of EB across the T_{COMP} [18–20]. However, microscopic and mesoscopic understanding of these two phenomena viz. NM and EB in the present compound is still lacking. We recall that no such NM and EB phenomena are exhibited by YCrO_3 [23,24], where Y^{3+} is a nonmagnetic ion, an isostructural compound to YbCrO_3 . It indicates the possible roles of $\text{Yb}^{3+}\text{-Cr}^{3+}$ or $\text{Yb}^{3+}\text{-Yb}^{3+}$ magnetic interactions in inducing the NM and EB phenomena in the YbCrO_3 compound. In this paper, we investigate the possible mechanism behind NM and EB phenomena in the YbCrO_3 compound by carrying out detailed microscopic neutron diffraction (ND), mesoscopic neutron depolarization, macroscopic (dc and ac) magnetization, specific heat, and dielectric studies. Field-cooled cooling (FCC) and field-cooled warming (FCW) modes of measured dc magnetization reveal that the compound exhibits NM with a T_{COMP} of 16.5 K. From low-temperature ND study under zero magnetic field on the present compound, we have shown that, at 120 K (T_N), Cr^{3+} orders into a *G*-type AFM configuration along the *z* axis, and in addition, a small polarized Yb^{3+} ordered moment down to 1.5 K is also evident from ND. Slightly negative thermal expansion (NTE) behavior along *a* and *b* axes was attributed to an increasing distance between Cr-Cr atoms lying in the *ab* plane below the T_{COMP} . Monotonic increase in ac susceptibility at low temperatures account for the polarized state of Yb^{3+} spin, which is in complete agreement with present ND and specific heat studies. Neutron depolarization study sheds light on the zero domain-magnetization state at $T \sim T_{\text{COMP}}$. Isothermal field-cooled (FC) magnetization $M(H)$ curves reveal the sign reversal of EB across the T_{COMP} . Interestingly, the compound exhibits anomalous behavior of coercivity and remanent magnetization in the vicinity of T_{COMP} . In addition to magnetic properties, dielectric properties are also studied to investigate the magnetoelectric coupling in the present YbCrO_3 compound.

II. EXPERIMENTAL DETAILS

Polycrystalline compound YbCrO_3 was prepared by the standard solid-state reaction method with Yb_2O_3 (99.99%) and Cr_2O_3 (99.99%) as the starting chemicals. X-ray diffraction (XRD) was performed at room temperature to check the phase purity of the compound. The dc magnetization measurements were performed in FCC and FCW modes using a commercial vibrating sample magnetometer as a function of temperature (4–300 K) and different applied magnetic fields. The ac susceptibility measurement under 987 Hz frequency was carried out as a function of temperature down to 2 K using a commercial ac susceptibility setup. For EB measurements, the sample was cooled in the presence of magnetic field down to the measuring temperature, and then isothermal $M(H)$ hysteresis loops were recorded under ± 50 kOe magnetic field. Before every EB measurement, the sample was warmed to the PM state (200 K) for demagnetization. The one-dimensional neutron depolarization experiment was carried out in the temperature range of 2–300 K using the polarized neutron spectrometer at Dhruva reactor ($\lambda = 1.201$ Å), Trombay, Mumbai. For this experiment, the sample was first cooled from room temperature down to 2 K in the presence of 50 Oe magnetic field, and then transmitted neutron beam polarization (P_f) was measured in the warming cycle as a function of temperature keeping the same magnetic field on. The sample used for this experiment was in the form of a pellet (7.5 mm thickness) of cylindrical dimension. The temperature-dependent ND experiment (1.5–300 K) under zero magnetic field was carried out on powder diffractometers PD-1 ($\lambda = 1.094$ Å) and PD-2 ($\lambda = 1.2443$ Å) equipped with one-dimensional position-sensitive detectors at Dhruva reactor, Trombay, Mumbai. Here, low temperature has been achieved by using a ^4He cryostat. Specific heat measurement over a temperature range of 4–200 K was carried out using a commercial physical property measurement system. Low-temperature dielectric measurements were carried out using a commercial Novocontrol alpha impedance analyzer. For cooling the sample down to 5 K, a closed-cycle refrigerator with ^4He exchange gas was used. Temperature-dependent capacitance (dielectric) data were measured in the frequency range 10 Hz to 1 MHz and over the temperature range of 5–300 K.

III. RESULTS AND DISCUSSION

A. X-ray diffraction

Figure 1 shows the powder x-ray diffraction pattern of the YbCrO_3 compound recorded at room temperature. The diffraction pattern was analyzed with the Rietveld refinement [25] technique using FULLPROF software. All Bragg peaks have been indexed in the *Pbnm* space group, and no extra Bragg peak was detected, which indicates the single-phase formation of the compound. YbCrO_3 crystallizes in an orthorhombic crystal structure, and lattice constants derived from the Rietveld refinement are $a = 5.194$ Å(5), $b = 5.500(6)$ Å, and $c = 7.487(4)$ Å. The lattice constants match well with literature-reported values [18–20,26]. Derived crystal structure along with CrO_6 octahedra is shown in Fig. 1(b). Further structural details with varying sample temperature have been discussed in Sec. III B 3.

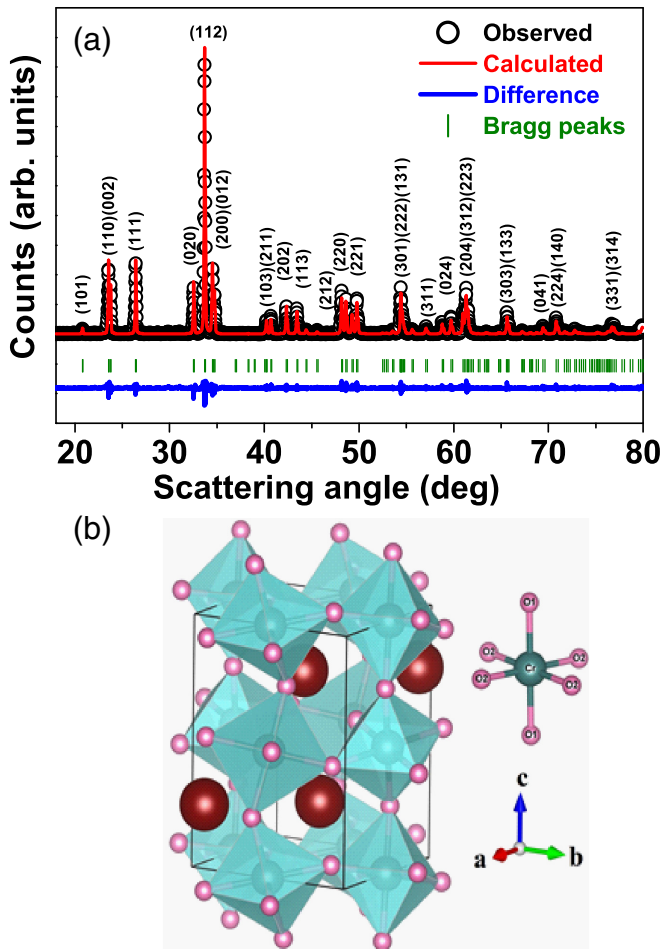


FIG. 1. Rietveld refined x-ray diffraction pattern of YbCrO₃ at 300 K. All Bragg peaks have been indexed with respective (hkl) values for the $Pbmm$ space group. The observed and calculated patterns are represented by black symbols and a solid red line, respectively. The difference pattern has been shown at the bottom by a blue line, while Bragg peaks have been shown by the vertical green lines. (b) Crystal structure of the YbCrO₃ compound along with CrO₆ octahedra. Here, O₁ is the apical oxygen along the c axis, while equatorial oxygen O₂ atoms lie in the ab plane.

B. Magnetic study

1. dc magnetization and ac susceptibility

Temperature (T) dependences of FCC dc magnetization (M) curves under various applied magnetic fields (H) are depicted in Fig. 2(a). As the temperature decreases from room temperature, the compound shows a magnetic ordering at $T_N \sim 120$ K. As we further decrease the temperature, magnetization increases and becomes maximum at $T \sim 70$ K. Interestingly, with further lowering of T , magnetization curves under $H \leq 1$ kOe show a downturn and approach to zero at the compensation temperature, T_{COMP} . The T_{COMP} value is 16.5 K for $H = 50$ Oe and matches well with previous literature reports [18–20]. At $T < T_{COMP}$, magnetization becomes negative and remains negative down to the lowest measured temperature of ~ 4 K. For $1 \text{ kOe} < H < 5 \text{ kOe}$, magnetization curves show a downturn below ~ 70 K, but net magnetization remains positive down to 4 K, while on the contrary, for

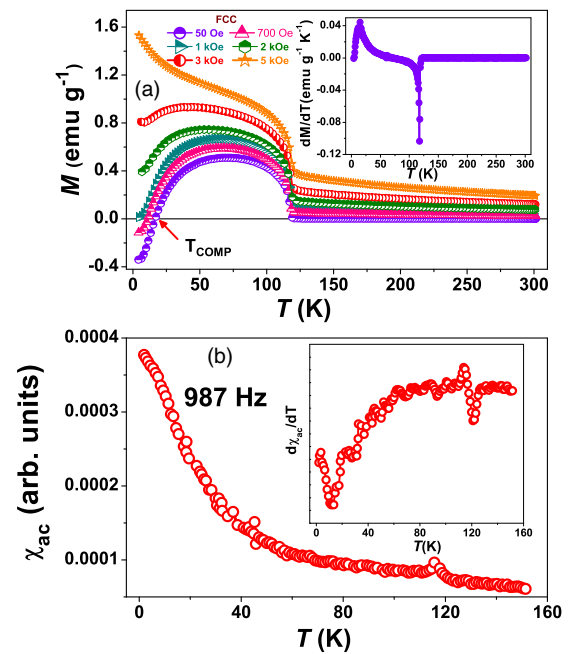


FIG. 2. (a) Field-cooled cooling (FCC) $M(T)$ curves recorded under various cooling magnetic fields. Inset shows the derivative of the dc magnetization curve measured under $H = 50$ Oe. (b) The real part of the ac susceptibility (χ_{ac}) measured at 987 Hz. Inset shows the $d\chi_{ac}/dT$ vs T curve.

$H \geq 5 \text{ kOe}$, $M(T)$ curves show a steep rise below 70 K. The derivative of the dc magnetization curve measured under 50 Oe magnetic field shows a minimum around the T_N and a peak at $T \sim 14$ K (close to T_{COMP} of 16.5 K). Both these anomalies at T_N and T_{COMP} are clearly visible in the real part of the ac susceptibility and its derivative curve, as shown in Fig. 2(b). Thus, macroscopic dc magnetization and ac susceptibility measurements are not sufficient to understand these anomalies in the YbCrO₃ compound. Therefore, experimental techniques, such as low-temperature neutron depolarization and ND, have been employed to understand the details of the low-temperature magnetic transition in the YbCrO₃ compound.

2. Neutron depolarization

Neutron depolarization is a mesoscopic probe, and it can measure the spatial magnetic inhomogeneity on a length scale from 100 Å to several microns [27–29]. In this experiment, a beam of polarized neutrons is passed through a sample. During the passage, magnetic induction of magnetic domains exerts a dipolar field on the neutron spin and depolarizes it owing to the Larmor precession in the local magnetic field of domains. Thus, a neutron depolarization experiment gives a good estimate of the net magnetization of the sample over the length scale of magnetic domains. The decrease in neutron beam polarization below $T < T_N$ suggests a magnetic ordering in YbCrO₃ with nonzero domain magnetization (Fig. 3). At $T \leq 70$ K [temperature at which dc magnetization becomes maximum, Fig. 2(a)], the neutron beam starts to gain its polarization, and full recovery is observed at $T \sim 20$ K (close to T_{COMP}). This indicates nearly zero domain magnetization in

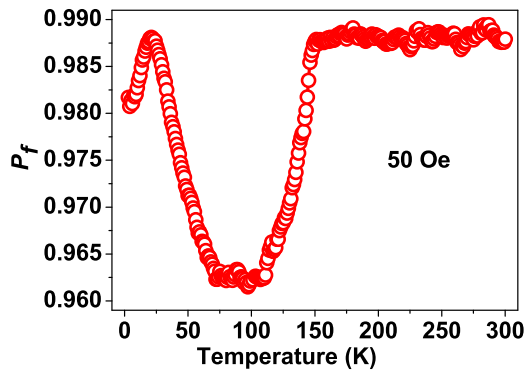


FIG. 3. Thermal variation of transmitted neutron beam polarization (P_f) under 50 Oe magnetic field for YbCrO_3 compound.

YbCrO_3 around the T_{COMP} . At $T < T_{\text{COMP}}$, the neutron beam gets depolarized again with lowering of temperature, indicating again a nonzero domain magnetization in the sample.

We have estimated the average domain size using the following relation:

$$P_f = P_i \exp[-\alpha(d/\delta)(\Phi_\delta)^2] \quad (1)$$

where P_i and P_f are the incident and transmitted neutron beam polarizations, α ($\sim \frac{1}{3}$) is a dimensionless parameter, d (~ 7.5 mm) is the effective thickness of the sample, and $\Phi_\delta = (4.63 \times 10^{-10} \text{ G}^{-1} \text{ \AA}^{-2}) \lambda B \delta$ is the precession angle per domain for a neutron of wavelength λ (1.201 \AA) travelling a distance δ (average domain size) in a domain magnetization B ($=4\pi M_s \rho$). Here, M_s and ρ are the saturation magnetization and density of the sample in emu g^{-1} and g cm^{-3} , respectively. Domain magnetization B at 5 K was estimated to be 283.24 G by using $M_s = 2.65 \text{ emu g}^{-1}$ and $\rho = 8.48 \text{ g cm}^{-3}$. Here, M_s was obtained from the zero FC $M(H)$ curve (not shown) at 5 K after subtracting the AFM contribution [30]. Using these values in Eq. (1), an average domain size $\delta \sim 0.94(4) \mu\text{m}$ at 5 K has been estimated.

To reveal the microscopic origin of magnetic transition in YbCrO_3 for $T < 20 \text{ K}$, Cr^{3+} and Yb^{3+} sublattice moments have been measured from temperature-dependent ND data under zero magnetic field.

3. Neutron diffraction

To determine the magnetic structure and variation of structural parameters in the YbCrO_3 compound, ND patterns at various temperatures (1.5–300 K) under zero magnetic field have been recorded. To determine the magnetic structure of YbCrO_3 , we have obtained the propagation vector \mathbf{K} by using the K-SEARCH program of the FULLPROF suite [25]. This program gives $\mathbf{K} = (000)$, which is suitable for finding the magnetic structure of the $R\text{CrO}_3$ family, and it remains unchanged in YbCrO_3 for $T \leq T_N$. The propagation vector describes the moment orientations of equivalent magnetic atoms in different nuclear cells. We have refined our ND data in the PM phase, i.e., $T > T_N$ by varying scale factor, zero shift, instrumental parameters, atomic positions, occupancies, lattice constants, and isotropic thermal parameters (B). Based on the Rietveld refined ND data in the PM phase, full occupancies of Yb^{3+} , Cr^{3+} , and O^{2-} ions at their respective sites

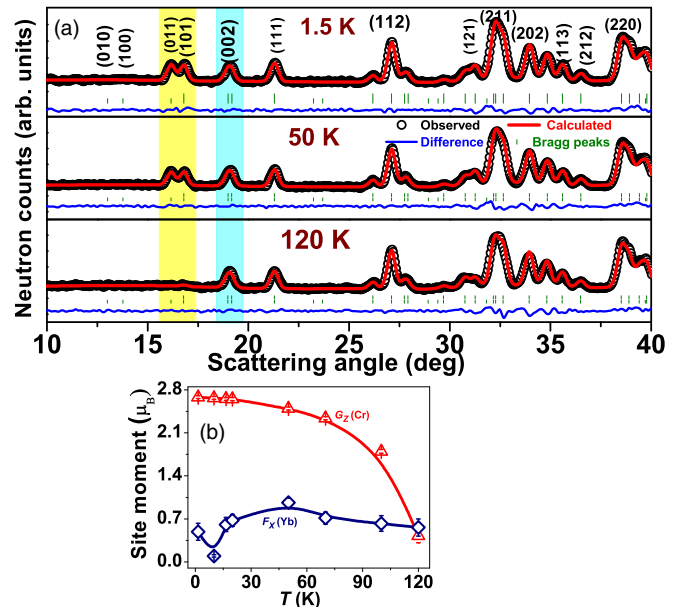


FIG. 4. (a) Rietveld refined neutron diffraction patterns at various temperatures. All Bragg peaks have been indexed with respective (hkl) values. The observed and calculated data are shown by black symbols and a solid red line, respectively. The difference of these two patterns is shown at the bottom by a blue line. The upper and lower vertical lines (green) represent the position of nuclear and magnetic Bragg peaks, respectively. The low angle magnetic and nuclear-cum-magnetic Bragg peaks are shown by the shaded area. Here, data have been recorded in the angular range of $3^\circ < 2\theta < 130^\circ$, but for clarity, only data up to $2\theta = 40^\circ$ are shown. (b) Thermal variations of G_z (Cr) and F_x (Yb) magnetic moments.

have been obtained. Consequently, we fixed the occupancies of these ions in the refinement of ND data at $T \leq T_N$, where only scale factor, atomic positions, lattice constants, atomic moments, and isotropic thermal parameters were refined.

The Rietveld refined ND patterns at some of the selected temperatures are depicted in Fig. 4(a). Structural parameters obtained from the ND refinement are listed in Table I. For comparison, parameters obtained from the Rietveld refinement of the XRD pattern at 300 K are also listed. It is evident from Fig. 4(a) that, at $T < T_N$ ($\sim 120 \text{ K}$), a new Bragg peak (011) at $2\theta = 16.16^\circ$ appears. The other Bragg peak (101) with strong magnetic contribution at $2\theta = 16.80^\circ$ has a very small nuclear contribution also. In addition to this, enhancement in intensity of the Bragg peak (002) at $2\theta = 18.97^\circ$ is also observed.

Now we discuss the magnetic structure of the YbCrO_3 compound using crystal symmetry arguments. Orthochromites crystallize in the $Pbnm$ space group, and transition metal ions occupy the $4b$ crystallographic site at positions $(\frac{1}{2}, 0, 0)$, $(\frac{1}{2}, 0, \frac{1}{2})$, $(0, \frac{1}{2}, \frac{1}{2})$, and $(0, \frac{1}{2}, 0)$. The irreducible representations in Bertaut notation [31] associated with the $4b$ site are $\Gamma_1(A_x, G_y, C_z)$, $\Gamma_3(G_x, A_y, F_z)$, $\Gamma_5(F_x, C_y, G_z)$, and $\Gamma_7(C_x, F_y, A_z)$. On the other hand, rare earth ions occupy the $4c$ crystallographic site at positions $(x, y, \frac{1}{4})$, $(\bar{x}, \bar{y}, \frac{3}{4})$, $(\frac{1}{2} + x, \frac{1}{2} - y, \frac{3}{4})$, and $(\frac{1}{2} - x, \frac{1}{2} + y, \frac{1}{4})$, and corresponding irreducible representations are $\Gamma_1(C_z)$, $\Gamma_2(A_x, G_y)$, $\Gamma_3(F_z)$, $\Gamma_4(G_x, A_y)$, $\Gamma_5(F_x, C_y)$, $\Gamma_6(G_z)$,

TABLE I. Structural parameters obtained from the Rietveld refinements of powder XRD at 300 K and powder ND data at 300 and 1.5 K. Here, O1 is the apical oxygen atom, and O2₁ and O2₂ are the equatorial oxygen atoms lying in the *ab* plane.

	XRD (300 K)	ND (300 K)	ND (1.5 K)
<i>a</i> (Å)	5.194 (5)	5.197 (6)	5.187 (3)
<i>b</i> (Å)	5.500 (6)	5.501 (9)	5.494 (4)
<i>c</i> (Å)	7.487 (4)	7.480 (11)	7.470 (6)
Fractional coordinates			
Yb (4 <i>c</i>)			
<i>x</i>	-0.0194 (2)	-0.0199 (1)	-0.0196 (2)
<i>y</i>	0.0688 (5)	0.0695 (8)	0.0714 (9)
<i>z</i>	0.2500	0.2500	0.2500
Cr (4 <i>b</i>)			
<i>x</i>	0.5000	0.5000	0.5000
<i>y</i>	0.0000	0.0000	0.0000
<i>z</i>	0.0000	0.0000	0.0000
O1 (4 <i>c</i>)			
<i>x</i>	0.1146 (11)	0.1123 (15)	0.1130(8)
<i>y</i>	0.4555 (12)	0.4585 (11)	0.4586 (15)
<i>z</i>	0.2500	0.25000	0.2500
O2 (8 <i>d</i>)			
<i>x</i>	-0.3111 (15)	-0.3097 (16)	-0.3103 (14)
<i>y</i>	0.3102 (9)	0.3036 (11)	0.3040 (12)
<i>z</i>	0.0544 (3)	0.0577 (5)	0.0565 (7)
Isotropic thermal parameters (Å ²)			
<i>B</i> _{Yb}	0.292 (15)	0.322 (19)	0.106 (17)
<i>B</i> _{Cr}	0.271 (25)	0.326 (35)	0.117 (54)
<i>B</i> _{O1}	0.421 (35)	0.424 (40)	0.362 (45)
<i>B</i> _{O2}	0.521 (30)	0.468 (32)	0.321 (26)
Bond length (Å)			
Cr-O1	1.973 (2)	1.975 (2)	1.970 (1)
Cr-O2 ₁	1.967 (5)	1.989 (3)	1.984 (4)
Cr-O2 ₂	2.009 (3)	1.986 (5)	1.982 (4)
Bond angle (deg)			
Cr-O1-Cr	142.051 (6)	142.988 (6)	142.787 (10)
Cr-O2-Cr	144.098 (8)	144.354 (8)	144.557 (4)
χ ²	1.56	3.14	3.11

$\Gamma_7(C_x, F_y)$, and $\Gamma_8(A_z)$. The best fit (lower R_{mag}) of the present ND data at $T \leq T_N$ has been obtained using $\Gamma_5(F_x^{\text{Cr}}, C_y^{\text{Cr}}, G_z^{\text{Cr}}, F_x^{\text{Yb}}, C_y^{\text{Yb}})$ representation [Fig. 4(a)] with finite G_z^{Cr} and F_x^{Yb} moments. Here, G_z^{Cr} is the AFM Cr³⁺ sublattice moment, which gives intensity corresponding to additional {(011) and (101)} Bragg peaks below the T_N , consistent with a previous literature report [3], whereas F_x^{Yb} is the polarized FM Yb³⁺ moment which accounts for the enhanced intensity of the (002) nuclear-cum-magnetic Bragg peak. It is necessary to include a finite moment for Yb³⁺ (F_x^{Yb}) in addition to G_z^{Cr} to get good agreement between the observed and calculated ND data. For instance, at 1.5 K (50 K), R_{mag} is ~ 6.40 (3.30) by considering both G_z^{Cr} and F_x^{Yb} components in comparison with $R_{\text{mag}} \sim 7.40$ (4.50) considering only the G_z^{Cr} component. Further, no finite intensities corresponding to the C_y component of both Cr³⁺ and Yb³⁺ sublattices and the F_x component of Cr³⁺ are seen in the present ND data of the YbCrO₃ compound. It is reported that the FM component of canted AFM Cr³⁺ (F_x^{Cr}) in $R\text{CrO}_3$ compounds is of the

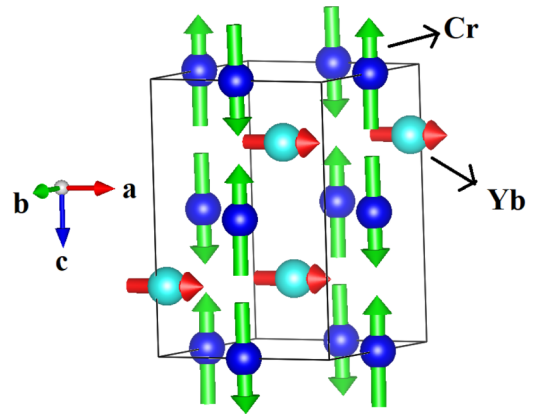


FIG. 5. Schematic representation of the magnetic structure of the YbCrO₃ compound as obtained from neutron diffraction study at 1.5 K.

order of 10^{-2} to $10^{-5} \mu_B$ [32]. For instance, Salazar-Rodriguez *et al.* [33] have reported $F_x^{\text{Cr}} \sim 0.013 \mu_B$ at 2 K in YCrO₃, an isostructural compound to the present YbCrO₃. This small F_x^{Cr} in the YbCrO₃ compound cannot be measured with certainty from the present ND data. However, the presence of the F_x^{Cr} moment is evident from our dc magnetization data below T_N [Fig. 2(a)]. Temperature variations of G_z^{Cr} and F_x^{Yb} moments are shown in Fig. 4(b). The G_z^{Cr} moment increases monotonically with decrease in temperature, showing a Brillouin function dependence with temperature. However, the F_x^{Yb} moment increases continuously until 50 K, which is close to the temperature for maximum EB (discussed later) and maximum magnetization [Fig. 2(a)]. At $T < 50$ K, the F_x^{Yb} moment decreases down to 10 K, and a small increment is observed at $T < 10$ K. This small increment in the F_x^{Yb} moment accounts for observed anomalies in derivatives of the dc and ac susceptibility data and depolarization of the neutron beam at $T < 20$ K. The magnetic structure of the YbCrO₃ compound at 1.5 K is depicted in Fig. 5. In next section, we have used the model of Cooke *et al.* [34] to explain observed NM in the present YbCrO₃ compound where the weak FM component of Cr³⁺ (M_{Cr}) and the polarized Yb³⁺ (M_{Yb}) moments are fitted to the temperature-dependent dc magnetization across the T_{COMP} .

Figure 6 shows temperature variations of the lattice constants, unit cell volume, and interatomic Cr-Cr distances via the oxygen atom. Lattice constant *a* decreases continuously until 20 K. At $T < 20$ K, lattice constant *a* shows an abrupt increase, indicating NTE behavior. Similar NTE behavior is observed along *b* at $T < 10$ K. However, the lattice constant *c* decreases monotonically with decrease in temperature down to 1.5 K. The unit cell volume *V* as a result shows small NTE behavior below ~ 10 K.

To understand the origin of NTE behavior in the YbCrO₃ compound, interatomic distances between Cr³⁺ atoms via O1 (apical oxygen along the *c* axis) and O2 (equatorial oxygen in the *ab* plane) were derived at various temperatures. It was found that the Cr-Cr distance via O1 decreases monotonically with decrease in temperature; however, the Cr-Cr distance via O2 shows an abrupt rise at $T < 20$ K.

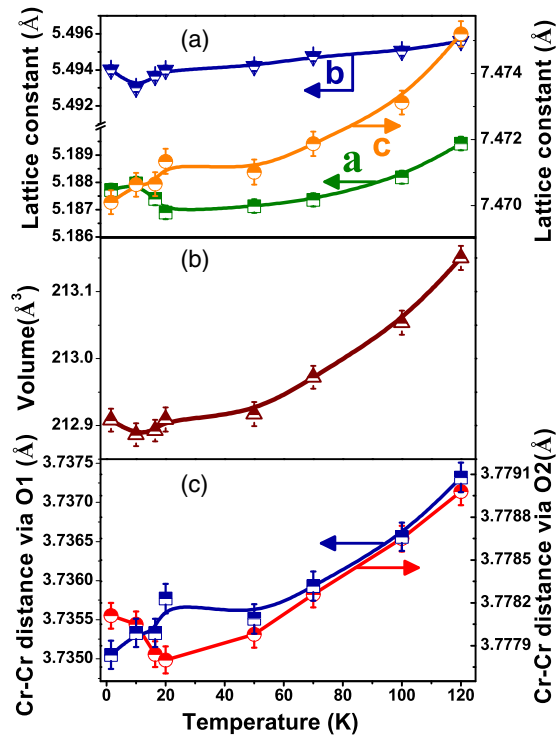


FIG. 6. Thermal variations of the (a) lattice constants, (b) unit cell volume, and (c) Cr-Cr distance via O1 (along the c direction) and O2 (in the ab plane), respectively. The solid lines are guides to the eye.

This explains the monotonic decrease of lattice constant c and NTE along a and b axes. Here, observed NTE in the YbCrO_3 compound is $\sim 0.08\%$, which might be assigned to magnetoelastic/magnetovolume effect produced by the repulsion between neighboring chromium ions. A similar kind of variation in lattice constants has been observed for the $\text{YbCr}_{0.5}\text{Fe}_{0.5}\text{O}_3$ compound [35].

4. Negative magnetization

In the literature, there are various kind of magnetic systems, such as garnets [36], spinels [37], orthovanadates [38], orthoferrites [39], and intermetallic alloys [10], which show the phenomenon of NM. However, the origin of the NM in different systems is different. The present compound YbCrO_3 also shows this phenomenon [Fig. 2(a)] below 16.5 K. Now we will give a possible explanation of the observed NM phenomenon in this compound. The Rietveld analysis of ND patterns at various temperatures indicates that a small and polarized Yb^{3+} moment [Fig. 4(b)] persists down to 1.5 K. A linear increase in ac susceptibility [Fig. 2(b)] below ~ 40 K also indicates the polarized nature of Yb^{3+} spins. Now we consider the role of the polarized moment of the rare earth ion (Yb^{3+}) to the observed NM in the YbCrO_3 compound. The NM in the present compound can be explained by considering the AFM coupling between the polarized Yb^{3+} moment (M_{Yb}) and the FM component of the Cr^{3+} moment (M_{Cr}), as explained in the case of other orthochromites [40–42]. The Yb^{3+} sublattice experiences an internal field due to ordered Cr^{3+} sublattice

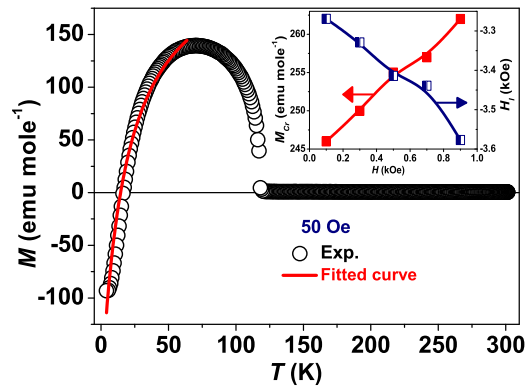


FIG. 7. M vs T curve measured under 50 Oe magnetic field. Solid line is the fitted curve as per the model proposed by Cooke *et al.* [34]. Inset shows the variation of M_{Cr} and H_I as a function of applied magnetic field, where solid lines are guides to the eye.

below the T_N . We have estimated the magnitude and sign of the internal field by fitting the magnetization across the T_{COMP} in the YbCrO_3 compound by the model proposed by Cooke *et al.* [34]. According to this model, temperature dependence of the magnetization (M) under some applied magnetic field (H) for $T < 70$ K can be fitted to the following equation:

$$M = M_{\text{Cr}} + C_{\text{Yb}} \frac{(H + H_I)}{T + \theta}, \quad (2)$$

where M_{Cr} is the FM component of canted Cr^{3+} sublattice, C_{Yb} is the Curie constant of Yb^{3+} , θ is the Curie-Weiss constant, H_I and H are the internal and applied magnetic fields, respectively. The value of the Curie constant is $2.576 \text{ emu K Oe}^{-1} \text{ mole}^{-1}$, as determined from effective moment of the Yb^{3+} ion ($\mu_{\text{eff}} \sim 4.54 \mu_B$). The M vs T curves for $H \leq 1 \text{ kOe}$ have been fitted with Eq. (2), and one of the fitted curves is shown in Fig. 7. The variations of derived parameters M_{Cr} and H_I with applied magnetic field are shown in the inset of Fig. 7. Here, M_{Cr} and $|H_I|$ are found to increase with the increase of applied magnetic field, a behavior observed in other orthochromites as well [40–42]. The negative value of H_I highlights its direction against the applied magnetic field as well as M_{Cr} . At $T < T_{\text{COMP}}$, M_{Yb} polarizes more and more in a direction opposite to M_{Cr} and becomes greater than M_{Cr} , resulting in NM. Similar explanations for the NM in TmCrO_3 [15] and $\text{NdCr}_{1-x}\text{Mn}_x\text{O}_3$ [41] compounds have been given in the literature.

5. Exchange bias

The temperature variations of magnetization for $H \leq 1 \text{ kOe}$ reveal the NM phenomenon in the present compound. When a compound shows NM and exhibits a sign reversal of EB across the T_{COMP} , it may be useful for many technological applications [17]. Therefore, it is of great interest to explore EB in the present compound. To understand the EB behavior, we have recorded isothermal $M(H)$ hysteresis loops at various temperatures in the range of 5–125 K, i.e., $T < T_N$ under cooling magnetic field (H_{COOL}) of 10 kOe. Some of the recorded hysteresis curves are shown in Fig. 8(a), and the thermal variation of the derived coercive field (H_C) from

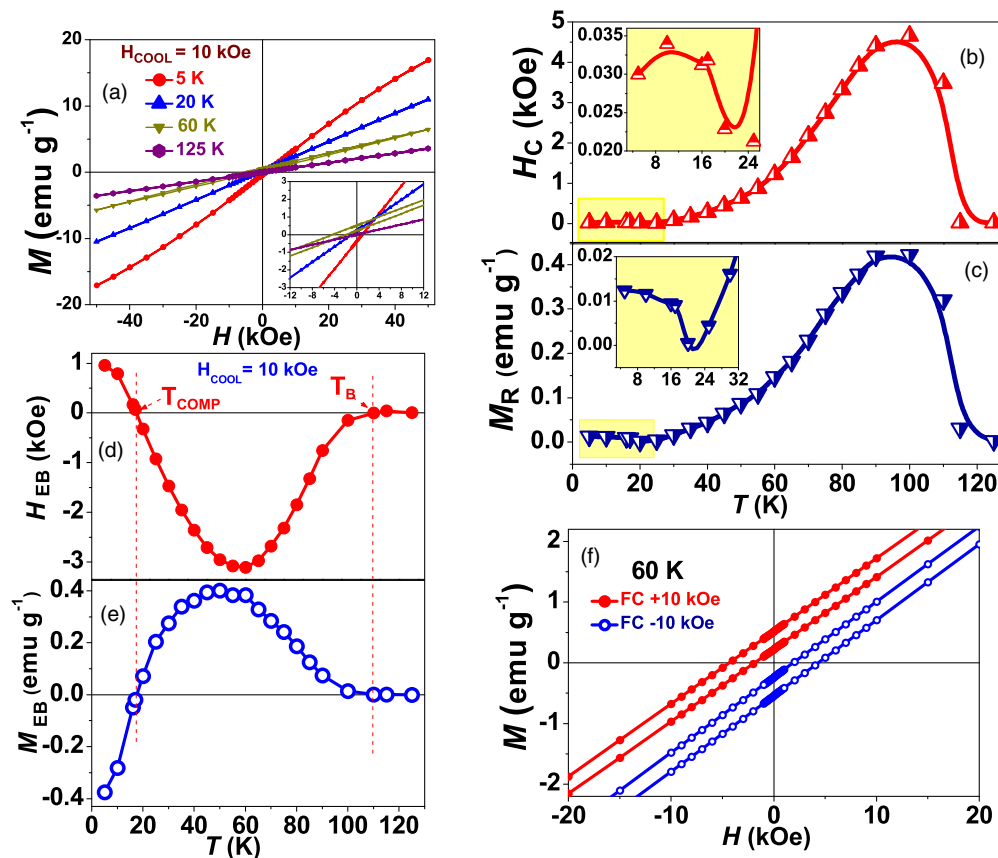


FIG. 8. (a) Measured field-cooled (FC) $M(H)$ curves under $H_{\text{COOL}} = 10$ kOe at various temperatures. Inset shows the enlarge view of the $M(H)$ curves at low magnetic fields. (b) and (c) Nonmonotonic variation of H_C and M_R with temperature. Inset shows the enlarge views of H_C and M_R in low temperature range. (d) and (e) Thermal variations of H_{EB} and M_{EB} . (f) $M(H)$ curves recorded at 60 K under $H_{\text{COOL}} = \pm 10$ kOe. The measurement range was ± 50 kOe. For clarity, only the data for ± 20 kOe are shown.

$M(H)$ loops is depicted in Fig. 8(b). The H_C is defined as $H_C = |H_{C1} - H_{C2}|/2$, where H_{C1} and H_{C2} are the left and right coercive fields in $M(H)$ curves. Below $T_N \sim 120$ K, H_C increases and reaches its maximum value at $T \sim 110$ K. Further, at $T < 110$ K, it decreases and shows a minimum (240 Oe) at $T \sim 20$ K (close to T_{COMP}). Below 20 K, H_C again increases with a value of 320 Oe at 5 K.

It is known that, in RCrO_3 orthochromites, various kinds of interactions among rare earth and transition metal ions, such as $\text{Cr}^{3+}\text{-Cr}^{3+}$, $\text{R}^{3+}\text{-Cr}^{3+}$, and $\text{R}^{3+}\text{-R}^{3+}$, influence the magnetic properties. Just below the T_N , $\text{Cr}^{3+}\text{-Cr}^{3+}$ interaction dominates, and in the liquid helium temperature range, $\text{R}^{3+}\text{-R}^{3+}$ interaction dominates. On the other hand, $\text{R}^{3+}\text{-Cr}^{3+}$ interaction plays an important role in the intermediate temperature range. Thus, it is the $\text{Yb}^{3+}\text{-Cr}^{3+}$ interaction which is responsible for the observed H_C behavior in the measured temperature range of $T < T_B$ (blocking temperature, a characteristic temperature other than T_{COMP} at which EB becomes zero). Here, it is noticed that not only the superexchange coupling between Yb^{3+} and Cr^{3+} spins contributes to the observed H_C , but the FM Cr^{3+} moment also plays an important role. Similar behavior of H_C has been reported for GdCrO_3 , where a sharp increase in H_C (~ 400 Oe) at $T < 10$ K was observed [43,44]. This rise in H_C was attributed to the AFM coupling between $\text{Gd}^{3+}\text{-Gd}^{3+}$ spins. However, for the present YbCrO_3 com-

pound, an increase in H_C at $T < 20$ K (close to T_{COMP}) is very small ~ 80 Oe. This small increase in H_C might be due to the increasing polarized Yb^{3+} moment, as evidenced by dc magnetization data (see Sec. III B 4). The remanent magnetization (M_R) follows the same temperature dependence [Fig. 8(c)] as that of H_C . The M_R is defined as $M_R = |M_{R1} - M_{R2}|/2$, where M_{R1} and M_{R2} are the remanent magnetization values corresponding to $H = 0$ during the ascending and descending branches of an $M(H)$ loop, respectively. Here, we have shown this kind of anomalous behavior of H_C and M_R for the YbCrO_3 compound. However, similar behavior has been observed in the Ru-doped YbCrO_3 compound [19].

Further, it has been observed in Fig. 8(a) that, for $T < T_{\text{COMP}}$ (16.5 K), $M(H)$ loops shift toward positive magnetic field and negative magnetization axes, and for $T > T_{\text{COMP}}$, $M(H)$ loops shift toward negative magnetic field axis and positive magnetization axes. It suggests a crossover from PEB to NEB across the T_{COMP} in YbCrO_3 . The EB field values are derived by the following relation:

$$H_{\text{EB}} = \frac{H_{C1} + H_{C2}}{2} \quad \text{and} \quad M_{\text{EB}} = \frac{M_{R1} + M_{R2}}{2}. \quad (3)$$

The temperature variations of H_{EB} and M_{EB} are shown in Figs. 8(d) and 8(e). For $T < T_{\text{COMP}}$, H_{EB} is found to be positive. With the increase in temperature, H_{EB} decreases and

becomes zero at T_{COMP} and finally becomes negative at $T > T_{\text{COMP}}$. After that, $|H_{\text{EB}}|$ increases and becomes maximum at $T \sim 60$ K (a temperature close to the point of maximum magnetization). Then it starts to decrease and becomes zero at $T_{\text{B}} \sim 110$ K, which is quite close to the temperature at which H_{C} exhibits a maximum [Fig. 8(b)]. Such a crossover of EB across the T_{COMP} has been reported for other Cr-based orthochromites [40,41] and also in intermetallic compounds [10].

The sign reversal of H_{EB} could be attributed to the competition between M_{Cr} and M_{Yb} moments across the T_{COMP} . For $T < T_{\text{COMP}}$, M_{Yb} dominates over M_{Cr} , as discussed earlier while describing the NM (Sec. III B 4). This facilitates an easy (hard) switching of magnetization from positive (negative) to negative (positive) in the FC hysteresis loop, resulting in a positive EB. PEB has been reported in the literature also [30,45,46]. For $T_{\text{COMP}} < T < T_{\text{N}}$, magnetocrystalline anisotropy increases with increasing temperature [see Fig. 8(b)], so Cr^{3+} will pin more and more the polarized Yb^{3+} moment. Thus, an extra negative magnetic field is required to switch the Yb^{3+} moment in the direction of the applied magnetic field. This causes the $M(H)$ loop to shift toward the negative horizontal axis of the magnetic field, and thus, NEB appears. The temperature dependence of M_{EB} [Fig. 8(e)] is like H_{EB} , except for $T < T_{\text{COMP}}$, M_{EB} is negative, while for $T > T_{\text{COMP}}$, it is positive. Now we discuss a possible explanation for the vertical shift, i.e., M_{EB} in the hysteresis loops. Various heterostructures, such as FM/spin-glass and FM/AFM interfaces exhibit M_{EB} , which has been driven by different mechanisms. For example, in FM/spin-glass systems [8], M_{EB} arises due to the frozen uncompensated FM spins at the FM/spin-glass interface. In the $\text{Co}/\text{Ca}_2\text{Ru}_{0.98}\text{Fe}_{0.02}\text{O}_4$ heterostructure [9], M_{EB} arises due to the FM contribution of canted Ru (Fe) moments. In the present compound, Cr^{3+} sublattice exhibits a canted AFM configuration, as evidenced by the macroscopic dc magnetization measurements. Therefore, FM Cr^{3+} spins might be responsible for the observed M_{EB} in the YbCrO_3 compound.

The isothermal $M(H)$ loops shown in Fig. 8(a) were recorded at various temperatures in the following protocol (known as P type): (+50 kOe) \rightarrow (0 kOe) \rightarrow (-50 kOe) \rightarrow (0 kOe) \rightarrow (+50 kOe). To confirm the conventional EB behavior of the compound, we have recorded the $M(H)$ loops at 60 K in another protocol (known as N type): (-50 kOe) \rightarrow (0 kOe) \rightarrow (+50 kOe) \rightarrow (0 kOe) \rightarrow (-50 kOe), as shown in Fig. 8(f). Here, the maximum applied field (H_{MAX}) to record a $M(H)$ curve in the P- and N-type protocols was 50 kOe. In the N-type protocol, both horizontal and vertical shifts of the $M(H)$ loop exist, and H_{EB} for this protocol is 3.10 kOe, which is close to the H_{EB} value at 60 K in the P-type protocol. This symmetric shift of the $M(H)$ loop in the opposite directions for the P- and N-type protocols implies the intrinsic nature of the EB in this compound, and thus, the possibility of the minor loop [47] effect has been excluded. Additionally, we have considered another approach to exclude the possibility of the minor loop effect. If the anisotropy field (H_{A}) of the compound is less than the maximum applied field (H_{MAX}), then the system should show a genuine or conventional EB. To calculate the H_{A} , we have used the law of approach to saturation magnetization method on the virgin curve of the

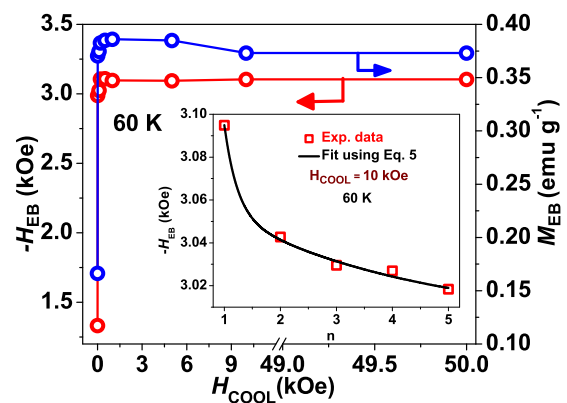


FIG. 9. Variation of $-H_{\text{EB}}$ and M_{EB} at 60 K with H_{COOL} . Inset shows the dependence of $-H_{\text{EB}}$ on the number of hysteresis loops (n) recorded under $H_{\text{COOL}} = 10$ kOe at 60 K. Square (red) symbol shows the experimental data, and solid black line is a fit to the experimental data.

$M(H)$ loop [48] at 5 K as given below:

$$M = M_S \left(1 - \frac{a}{H} - \frac{b^2}{H^2} \right) + \chi_F H, \quad (4)$$

where a and b are the constant parameters, M_S is the saturation magnetization, and χ_F is the high field susceptibility. Here, parameter $b = 4K^2/15M_S^2$ gives the measure of magnetocrystalline anisotropy (where K is an anisotropic constant). Using these parameters, the value of H_{A} ($\sim 2K/M_S$) is determined to be ~ 21 kOe, which is comparable with the H_{A} values found in the single-layered Ruddlesden-Popper perovskite $\text{LaSrCo}_{0.5}\text{Mn}_{0.5}\text{O}_4$ [49] and $\text{LaMn}_{0.7}\text{Fe}_{0.3}\text{O}_3$ [50]. Thus, the derived value of H_{A} in the present compound is less than the H_{MAX} , which further indicates the absence of a minor loop effect.

To gain more insight into the EB phenomenon, we have recorded $M(H)$ loops under different cooling magnetic fields (H_{COOL}) at 60 K. Figure 9 demonstrates the effect of H_{COOL} on the EB fields at 60 K. No reversal of EB field was observed with varying H_{COOL} , as observed in temperature variation of EB parameters. At low H_{COOL} , not all M_{Cr} align in the direction of the applied field, so the exchange coupling is expected to be weak, and hence, H_{EB} is small. However, as H_{COOL} increases, more and more M_{Cr} align in the direction of the applied field. At $H_{\text{COOL}} \geq 0.5$ kOe, all M_{Cr} will be aligned in the direction of the applied field; consequently, exchange coupling gets saturated. Thus, saturation of M_{Cr} results in the observed saturation of the H_{EB} . Similar behavior of cooling field dependence of H_{EB} has been reported for $\text{NdCr}_{1-x}\text{Mn}_x\text{O}_3$ [40] and $\text{Dy}_{1-x}\text{Nd}_x\text{CrO}_3$ [51] compounds. Similarly, M_{EB} follows the same trend with H_{COOL} as that of H_{EB} . Since change in M_{EB} is very small ($\sim 2\%$), this suggests that the M_{Cr} does not change so much with increase of H_{COOL} .

Training effect (TE) is a complementary characteristic of H_{EB} , and it is manifested as a gradual decrease in H_{EB} when the system is cycled through several consecutive hysteresis loops [52]. We have done this measurement for five consecutive hysteresis loops at 60 K. It is found that H_{EB} decreases monotonically with increasing number of cycles (n), as shown

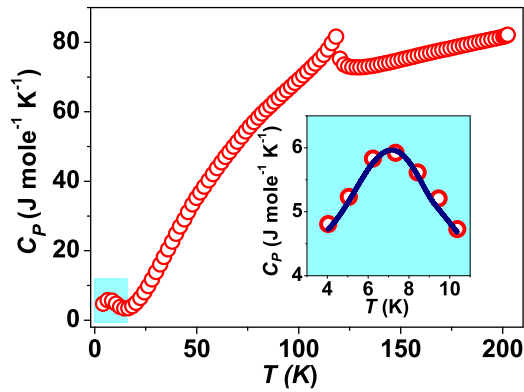


FIG. 10. Temperature dependence of the specific heat capacity (C_p) under zero applied magnetic field. Inset shows the fitting of low temperature hump as per Eq. (6).

in the inset of Fig. 9. The data were fitted with the following model [53]:

$$H_{EB}^n = H_{EB}^\infty + A_r \exp\left(\frac{-n}{P_r}\right) + A_f \exp\left(\frac{-n}{P_f}\right), \quad (5)$$

where H_{EB}^n is the EB field of the n th hysteresis loop, and A_r , A_f , P_r , P_f , and H_{EB}^∞ are the fitting parameters. Here, A_r and P_r are the parameters related to the rotatable AFM spins, while A_f and P_f correspond to the frozen AFM spins, respectively. The parameters obtained from the fitting are $H_{EB}^\infty = 3.002$ kOe, $A_r = 0.067$ kOe, $P_r = 3.5$, $A_f = 3.3$ kOe, and $P_f = 0.23$. These values are quite like the values obtained for $\text{La}_{0.15}\text{Pr}_{0.85}\text{CrO}_3$ [54] and the Ruddlesden-Popper perovskite $\text{LaSrCo}_{0.5}\text{Mn}_{0.5}\text{O}_4$ [49]. Since decrease of H_{EB} in YbCrO_3 is very small ($\sim 2.5\%$), it signifies a stable spin configuration against the cycling of hysteresis loops. This observation agrees with the cooling field dependence of EB fields (see the main panel of Fig. 9).

C. Specific heat capacity

Figure 10 shows the specific heat capacity [55] C_p of the YbCrO_3 compound under zero magnetic field in a temperature range of 4–200 K. A λ -shaped anomaly is observed at 120 K, which is associated with the canted AFM ordering (T_N) of Cr^{3+} moments, in agreement with other macroscopic as well as microscopic measurements on the YbCrO_3 compound. With decrease in temperature from T_N , C_p continuously decreases down to 15 K, close to T_{COMP} . Afterwards, it increases, and a small hump is observed centered at $T \sim 7$ K. This hump might be related to magnetic Yb^{3+} spins [56] since no such peak is present in specific heat data of YCrO_3 , where Y^{3+} ion is nonmagnetic [57]. Further, it may be noted that the λ -shaped anomaly showing magnetic ordering of rare earth ions due to R^{3+} - R^{3+} interaction is present in nonmagnetic B-site-based perovskite compounds such as NdGaO_3 and NdCoO_3 [58].

The hump in low-temperature C_p data for the YbCrO_3 compound could be attributed to the Schottky anomaly, which arises due to the polarized Yb^{3+} spins. We have fitted the low-temperature C_p data under zero magnetic field by considering the lattice and the Schottky term for a two-level system as

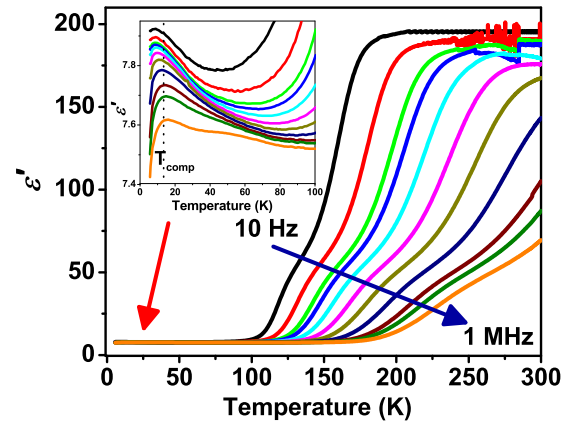


FIG. 11. Variation of real part of dielectric constant (ϵ') as a function of temperature at various frequencies. Inset shows the dielectric anomaly at T_{COMP} .

[59,60]

$$C_p(T) = a_1 T^3 + a_2 T^5 + a_3 T^7 + N \left(\frac{\Delta E}{k_B T} \right)^2 \left\{ \frac{\exp\left(\frac{\Delta E}{k_B T}\right)}{[1 + \exp\left(\frac{\Delta E}{k_B T}\right)]^2} \right\}. \quad (6)$$

Here, a_1 , a_2 , and a_3 are the lattice (phononic) specific heat parameters, N/R is the number of free spins with R as a universal gas constant, and ΔE is the energy gap for the Zeeman splitting of the Yb^{3+} doublet. The low-temperature hump in C_p data for the YbCrO_3 compound fits well with Eq. (6), as shown in the inset of Fig. 10, and the fitting parameters are $a_1 = 3.63 \times 10^{-2} \text{ J mole}^{-1} \text{ K}^{-3}$, $a_2 = -6.12 \times 10^{-4} \text{ J mole}^{-1} \text{ K}^{-5}$, $a_3 = 2.93 \times 10^{-6} \text{ J mole}^{-1} \text{ K}^{-7}$, $N = 8.66 \text{ J mole}^{-1} \text{ K}^{-1}$, and $\Delta E = 0.53 \text{ meV}$ ($\sim 6.1 \text{ K}$). The inset of Fig. 10 shows that our experimental data fitted well with Eq. (6). This indicates that the hump in C_p data of the YbCrO_3 compound comes from polarized Yb^{3+} spins, consistent with literature reports on YbFeO_3 [61,62], an isostructural compound to YbCrO_3 . Thus, the polarized Yb^{3+} moment in the present YbCrO_3 compound becomes significant at low temperatures ($< T_{\text{COMP}}$) and therefore plays an important role in dictating magnetic properties *viz.* the EB and MR.

D. Dielectric study

We have also performed temperature-dependent dielectric measurements in the frequency range of 1 Hz to 1 MHz. Figure 11 shows that, at any temperature, the real part of the dielectric constant (ϵ') decreases with increasing frequency, showing that YbCrO_3 has temperature-dependent Debye-like relaxations [63]. A shoulderlike feature is observed in 10 Hz spectra of ϵ' at $T \sim T_N$ and this shoulder shifts toward high temperature with increasing frequency. Moreover, ϵ' shows an anomaly at T_{COMP} , and this anomaly persists at all measured frequencies (see the inset of Fig. 11). This indicates the possible correlation between electric and magnetic properties in the YbCrO_3 compound. The observed dielectric anomaly at T_{COMP} indicates a weak magnetoelectric coupling in the YbCrO_3 compound. Such a magnetoelectric coupling has

been reported in other orthochromites also, where the interaction between magnetic rare earth and canted Cr ions is cited as one of the possible causes of such a coupling [64].

IV. SUMMARY AND CONCLUSIONS

In summary, we have investigated the origin of intertwined magnetization and EB reversals across T_{COMP} (~ 16.5 K) in the YbCrO_3 compound by carrying out dc magnetization, ac susceptibility, specific heat, ND, neutron depolarization, and dielectric measurements. The dc magnetization study is consistent with a canted AFM ordering of Cr^{3+} moments below T_{N} (~ 120 K) involving a weak FM component of magnetization (M_{Cr}). The observed Schottky anomaly in the specific heat data and monotonic increase of ac susceptibility at low temperatures are well accounted with a polarized nature of the Yb^{3+} moment (M_{Yb}). This polarization has been further confirmed by ND study, where a finite ordered moment for Yb^{3+} has been observed below T_{N} . Moreover, ND study infers the G_z -type AFM ordering of Cr^{3+} moments at low temperatures with $T_{\text{N}} \sim 120$ K, though the weak FM component (M_{Cr}) could not be measured due to the detection limitation of the ND technique. Interestingly, with decreasing temperature, NTEs of lattice constants a and b below the T_{COMP} have also been found. These NTEs are attributed to the increase in separation between Cr-Cr atoms via equatorial oxygen atoms lying in the ab plane below the T_{COMP} . The phenomenon of NM, observed in the present dc magnetization study, has been explained in terms of the competition between the antiparallely coupled M_{Yb} and M_{Cr} moments. In the FC dc magnetization measurement, the weak FM component of Cr^{3+} sublattice M_{Cr} gets aligned along the direction of the applied field, yielding a net positive magnetization in the temperature range $T_{\text{COMP}} < T < T_{\text{N}}$. At temperatures below the T_{COMP} , M_{Yb}

[aligned opposite to the applied field (H) and M_{Cr}] overtakes M_{Cr} , resulting in a net NM for the YbCrO_3 compound. Similarly, EB, arising due to the atomistic AFM coupling between M_{Yb} and M_{Cr} moments, also changes sign at the T_{COMP} . At $T > T_{\text{COMP}}$, the compound shows a usual positive magnetization behavior with a NEB. Below the T_{COMP} , while recording a FC $M(H)$ hysteresis loop with field decreasing from $H = +H_{\text{max}}$, a sign change of magnetization from positive to negative occurs at a relatively lower value of applied field (corresponding to a lower value of left coercivity H_{C1}). This happens because the NM state is favored at $T < T_{\text{COMP}}$, whereas extra magnetic field is required to change the sign of magnetization from negative to positive during the forward field cycle (i.e., over $H = -H_{\text{max}}$ to $+H_{\text{max}}$), as the magnetic state changes to a positive state, which is energetically unfavorable at $T < T_{\text{COMP}}$. This results in a relatively higher value of right coercivity (H_{C2}). For the present compound, both H_{C1} and H_{C2} are positive, and the EB is positive at $T < T_{\text{COMP}}$. Neutron depolarization study under 50 Oe magnetic field sheds more light on zero domain magnetization state at the T_{COMP} . An anomaly at $T \sim T_{\text{COMP}}$ in dielectric measurement indicates the possible correlation between electric and magnetic properties, i.e., a weak magnetoelectric coupling in the YbCrO_3 compound. The present understanding of magnetization and EB reversals across T_{COMP} in a single-phase compound and the observed magnetoelectric coupling may open the possibility for making thermomagnetic switches, spin-valve, electromagnetic, and other spintronic devices.

ACKNOWLEDGEMENT

The authors acknowledge S. K. Mishra for measuring the dielectric data.

-
- [1] A. Kumar and S. M. Yusuf, *Phys. Rep.* **556**, 1 (2015).
 [2] J. Prado-Gonjal, R. Schmidt, J.-J. Romero, D. Ávila, U. Amador, and E. Morán, *Inorg. Chem.* **52**, 313 (2013).
 [3] N. Shamir, H. Shaked, and S. Shtrikman, *Phys. Rev. B* **24**, 6642 (1981).
 [4] P. K. Manna and S. M. Yusuf, *Phys. Rep.* **535**, 61 (2014).
 [5] P. K. Manna, S. M. Yusuf, R. Shukla, and A. K. Tyagi, *Phys. Rev. B* **83**, 184412 (2011).
 [6] S. M. Yusuf, P. K. Manna, M. M. Shirolkar, S. K. Kulkarni, R. Tewari, and G. K. Dey, *J. App. Phys.* **113**, 173906 (2013).
 [7] P. K. Manna, S. M. Yusuf, R. Shukla, and A. K. Tyagi, *Appl. Phys. Lett.* **96**, 242508 (2010).
 [8] Y.-K. Tang, Y. Sun, and Z.-H. Cheng, *Phys. Rev. B* **73**, 174419 (2006).
 [9] S. J. Yuan, L. Li, T. F. Qi, L. E. DeLong, and G. Cao, *Phys. Rev. B* **88**, 024413 (2013).
 [10] S. Venkatesh, U. Vaidya, V. Rakhecha, S. Ramakrishnan, and A. Grover, *J. Phys. Condens. Matter* **22**, 496002 (2010).
 [11] A. Kumar, S. M. Yusuf, and C. Ritter, *Phys. Rev. B* **96**, 014427 (2017).
 [12] F. Hong, Z. Cheng, J. Wang, X. Wang, and S. Dou, *Appl. Phys. Lett.* **101**, 102411 (2012).
 [13] J. Mao, Y. Sui, X. Zhang, X. Wang, Y. Su, Z. Liu, Y. Wang, R. Zhu, Y. Wang, W. Liu, and X. Liu, *Solid State Commun.* **151**, 1982 (2011).
 [14] L. Wang, G. Rao, X. Zhang, L. Zhang, S. Wang, and Q. Yao, *Ceram. Int.* **42**, 10171 (2016).
 [15] K. Yoshii, *Mater. Res. Bull.* **47**, 3243 (2012).
 [16] B. B. Dash and S. Ravi, *J. Magn. Magn. Mater.* **461**, 91 (2018).
 [17] I. Prejbeanu, M. Kerekes, R. Sousa, H. Sibuet, O. Redon, B. Dieny, and J. Eres, *J. Phys. Condens. Matter* **19**, 165218 (2007).
 [18] Y. Su, J. Zhang, Z. Feng, L. Li, B. Li, Y. Zhou, Z. Chen, and S. Cao, *J. App. Phys.* **108**, 013905 (2010).
 [19] B. Dalal, B. Sarkar, V. Dev Ashok, and S. K. De, *J. Phys. Condens. Matter* **28**, 426001 (2016).
 [20] L. Wang, S. W. Wang, X. Zhang, L. L. Zhang, R. Yao, and G. H. Rao, *J. Alloys Compd.* **662**, 268 (2015).
 [21] P. Gupta and P. Poddar, *Inorg. Chem.* **54**, 9509 (2015).
 [22] S. Shtrikman, B. M. Wanklyn, and I. Yaeger, *Int. J. Magn.* **1**, 327 (1971).
 [23] D. Deng, J. Zheng, D. Yu, B. Wang, D. Sun, M. Avdeev, Z. Feng, C. Jing, B. Lu, W. Ren, S. Cao, and J. Zhang, *Appl. Phys. Lett.* **107**, 102404 (2015).

- [24] A. Durán, R. Escamilla, R. Escudero, F. Morales, and E. Verdín, *Phys. Rev. Materials* **2**, 014409 (2018).
- [25] H. Rietveld, *J. App. Crystallo.* **2**, 65 (1969).
- [26] J.-S. Zhou, J. A. Alonso, V. Pomjakhusin, J. B. Goodenough, Y. Ren, J-Q. Yan, and J-Q. Cheng, *Phys. Rev. B* **81**, 214115 (2010).
- [27] O. Halpern and T. Holstein, *Phys. Rev.* **59**, 960 (1941).
- [28] S. M. Yusuf, M. Sahana, K. Dörr, U. K. Rößler, and K. H. Müller, *Phys. Rev. B* **66**, 064414 (2002).
- [29] I. Dhiman, A. Das, R. Mittal, Y. Su, A. Kumar, and A. Radulescu, *Phys. Rev. B* **81**, 104423 (2010).
- [30] Deepak, A. Kumar, and S. M. Yusuf, *J. Appl. Phys.* **127**, 213903 (2020).
- [31] E. F. Bertaut, *Acta Cryst. A* **24**, 217 (1968).
- [32] I. Dzyaloshinsky, *J. Phys. Chem. Solids* **4**, 241 (1958).
- [33] R. Salazar-Rodriguez, D. Aliaga-Guerra, and K. M. Taddei, *Hyperfine Interact.* **240**, 82 (2019).
- [34] A. Cooke, D. Martin, and M. Wells, *J. Phys. C: Solid State Phys.* **7**, 3133 (2001).
- [35] F. Pomiro, R. D. Sánchez, G. Cuello, A. Maignan, C. Martin, and R. E. Carbonio, *Phys. Rev. B* **94**, 134402 (2016).
- [36] M. Ghanathe, A. Kumar, and S. M. Yusuf, *J. Appl. Phys.* **125**, 093903 (2019).
- [37] M. Ghanathe, A. Kumar, I. da Silva, and S. M. Yusuf, *J. Magn. Mater.* **523**, 167632 (2021).
- [38] Y. Ren, T. T. M. Palstra, D. I. Khomskii, E. Pellegrin, A. A. Nugroho, A. A. Menovsky, and G. A. Sawatzky, *Nat.* **396**, 441 (1998).
- [39] S. J. Yuan, W. Ren, F. Hong, Y. B. Wang, J. C. Zhang, L. Bellaiche, S. X. Cao, and G. Cao, *Phys. Rev. B* **87**, 184405 (2013).
- [40] T. Bora and S. Ravi, *J. App. Phys.* **116**, 063901 (2014).
- [41] T. Bora and S. Ravi, *J. Magn. Mater.* **386**, 85 (2015).
- [42] N. Sharma, B. K. Srivastava, A. Krishnamurthy, and A. K. Nigam, *Solid State Sci.* **12**, 1464 (2010).
- [43] A. Jaiswal, R. Das, K. Vivekanand, T. Maity, P. M. Abraham, S. Adyanthaya, and P. Poddar, *J. App. Phys.* **107**, 013912 (2010).
- [44] M. Tripathi, T. Chatterji, H. E. Fischer, R. Raghunathan, S. Majumder, R. J. Choudhary, and D. M. Phase, *Phys. Rev. B* **99**, 014422 (2019).
- [45] J. Nogués, J. Sorta, V. Langlaisb, V. Skumryeva, S. Suriñachb, J. S. Muñozb, and M. D. Baró, *Phys. Rep.* **422**, 65 (2005).
- [46] J. Nogués, D. Lederman, T. J. Moran, and I. K. Schuller, *Phys. Rev. Lett.* **76**, 4624 (1996).
- [47] A. Harres, M. Mikhov, V. Skumryev, A. M. H. de Andrade, J. E. Schmidt, and J. Geshev, *J. Magn. Mater.* **402**, 76 (2016).
- [48] S. V. Andreev, M. I. Bartashevich, V. I. Pushkarsky, V. N. Maltsev, L. A. Pamyatnykh, E. N. Tarasov, N. V. Kudrevatykh, and T. Goto, *J. Alloys and Compd.* **260**, 196 (1997).
- [49] R. R. Das, P. Parida, A. K. Bera, T. Chatterji, B. R. K. Nanda, and P. N. Santhosh, *Phys. Rev. B* **98**, 184417 (2018).
- [50] M. Patra, M. Thakur, K. De, S. Majumdar, and S. Giri, *J. Phys. Condens. Matter* **21**, 078002 (2009).
- [51] A. McDannald, C. R. dela Cruz, M. S. Seehra, and M. Jain, *Phys. Rev. B* **93**, 184430 (2016).
- [52] C. Binek, *Phys. Rev. B* **70**, 014421 (2004).
- [53] S. K. Mishra, F. Radu, H. A. Dürr, and W. Eberhardt, *Phys. Rev. Lett.* **102**, 177208 (2009).
- [54] K. Yoshii, *Appl. Phys. Lett.* **99**, 142501 (2011).
- [55] C. A. Martin, *J. Phys. Condens. Matter* **3**, 5967 (1991).
- [56] A. Muñoz, J. A. Alonso, M. T. Casais, M. J. Martínez-Lope, J. L. Martínez, and M. T. Fernández-Díaz, *J. Mater. Chem.* **13**, 1234 (2003).
- [57] Y. Su, L. Li, Z. Xing, Z. Feng, D. Deng, B. Kang, S. Cao, and J. Zhang, in *2011 International Symposium on Applications of Ferroelectrics (ISAF/PFM) and 2011 International Symposium on Piezoresponse Force Microscopy and Nanoscale Phenomena in Polar Materials* (IEEE, Vancouver, BC, 2011), pp. 1–4.
- [58] F. Bartolomé, M. D. Kuz'min, J. Bartolomé, J. Blasco, J. García, and F. Sapiña, *Solid State Commun.* **91**, 177 (1994).
- [59] S. J. Yuan, Y. M. Cao, L. Li, T. F. Qi, and S. X. Cao, *J. Appl. Phys.* **114**, 113909 (2013).
- [60] L. S. Wu, S. E. Nikitin, M. Brando, L. Vasylechko, G. Ehlers, M. Frontzek, A. T. Savici, G. Sala, A. D. Christianson, M. D. Lumsden, and A. Podlesnyak, *Phys. Rev. B* **99**, 195117 (2019).
- [61] M. R. Moldover, G. Sjolander, and W. Weymann, *Phys. Rev. Lett.* **26**, 1257 (1971).
- [62] E. Li, Z. Feng, B. Kang, J. Zhang, W. Ren, and S. Cao, *J. Alloys Compd.* **811**, 152043 (2019).
- [63] Z. Xiang, J. Xu, Y. Huang, S. Ge, and Y. Cui, *Prog. Nat. Sci.: Mater. Int.* **28**, 609 (2018).
- [64] B. Rajeswaran, D. I. Khomskii, A. K. Zvezdin, C. N. R. Rao, and A. Sundaresan, *Phys. Rev. B* **86**, 214409 (2012).